

mechanosensory cues. To identify the function of this additional behavior, eels were presented with prey hidden below a thin agar barrier (Fig. 3C). In some cases, eels detected prey through the barrier and attacked directly, but in other cases, the eel investigated the agar surface with a low-amplitude electric organ discharge and then produced a high-voltage doublet. The doublet invariably caused prey movement. Stimulated prey movement was closely followed (in 20 to 40 ms) by a full predatory strike consisting of a strong electric discharge volley and directed attack (Fig. 3 and movie S5), as characterized in the first experiments. The distinct form of the discharge trace in these trials consisted of a doublet (or triplet) followed by a 20- to 40-ms pause (during which prey moved) and then a full discharge volley (Fig. 3, D and F).

The results of the doublet experiment suggest that the eels may use doublet and triplet discharges to detect cryptic prey by inducing movement. To test this hypothesis, a pithed fish was placed in a thin plastic bag to isolate it from the eel's discharge. The electrically isolated fish was positioned below an agar barrier, with electrical leads embedded in the head and tail region (10) that allowed production of artificial fish twitch by the experimenter. Artificial fish twitch was triggered remotely through a stimulator (Fig. 4A), allowing control over its timing and occurrence. When the stimulating electrodes were inactive, eel doublets caused no response in the pithed fish and eels did not attack the preparation (Fig. 4B and movie S6). However, when the stimulator was configured to trigger fish twitch when the eel produced a doublet, the eel's full "doublet attack" behavior was replicated (Fig. 4C and movie S6). The attack pattern consisted of a doublet, followed by a short pause, during which the prey moved (resulting from the triggered stimulator), followed by a high-voltage volley and strike. This key experiment showed that eels never (10 of 10 trials for each of two eels) followed a doublet with an attack volley without a "mechanosensory echo" from the prey, but attacked in response to the stimulator-generated fish twitch (10 of 10 trials for each of two eels; $P < 0.0001$, binomial test). Experimenter-triggered twitches, in the absence of eel hunting doublets, also generated attacks (movie S6) with the time course observed above (Fig. 4D and supplementary materials). Thus, prey movement, whether doublet-generated or independently generated, elicited short latency (20 to 40 ms) attacks. Eels also appeared to use either active or passive electrolocation to detect live prey under agar and often attacked without a preceding doublet. But in no case did an attack volley follow a doublet in the absence of prey response. Thus, the doublet appears to answer the question, "Are you living prey?" when information is limited. Preliminary observations suggest that "doublet hunting" is most common in complex environments (movie S7). A range of controls confirmed that eels were responding to twitch-generated mechanosensory cues in this paradigm (Fig. 4 and movie S6).

Together, the results of these experiments show that high-voltage discharges of electric eels re-

motely activate motor neuron efferents in nearby animals. Prey that have been detected can be immobilized and captured. Hidden prey can be induced to twitch, revealing their location. The latter strategy, which often triggers an escape response, depends on the eel's short reaction time. An eel can discharge its high-voltage train 20 ms after a mechanosensory stimulus, allowing it to cancel the very escape response it has generated. Overall, this study reveals that the electric eel has evolved a precise remote control mechanism for prey capture, one that takes advantage of an organisms' own nervous system.

REFERENCES AND NOTES

1. H. Grundfest, *Prog. Biophys. Biop. Chem.* **1957**, 1–85 (1956).
2. S. Finger, M. Piccolino, *The Shocking History of Electric Fishes: From Ancient Epochs to the Birth of Modern Neurophysiology* (Oxford Univ. Press, Oxford, 2011), p. 5.
3. J. Keeseey, *J. Hist. Neurosci.* **14**, 149–164 (2005).
4. J. R. Gallant et al., *Science* **344**, 1522–1525 (2014).
5. R. Bauer, *Behav. Ecol. Sociobiol.* **4**, 311–319 (1979).
6. C. W. Coates, R. T. Cox, W. A. Roseblith, M. B. Brown, *Zoologica* **25**, 249 (1940).
7. S. Hagiwara, T. Szabo, P. S. Enger, *J. Neurophysiol.* **28**, 775–783 (1965).
8. T. H. Bullock, *Brain Behav. Evol.* **2**, 85–101 (1969).

9. G. M. Westby, *Behav. Ecol. Sociobiol.* **22**, 341–354 (1988).
10. Materials and methods are available as supplementary materials on Science Online.
11. A. J. Kalmijn, *J. Exp. Biol.* **55**, 371–383 (1971).
12. R. Hennig, T. Lomo, *Nature* **314**, 164–166 (1985).
13. K. K. Pedersen, O. B. Nielsen, K. Overgaard, *Physiol. Rep.* **1**, e00026 (2013).
14. A. J. Cheng, N. Place, J. D. Bruton, H. C. Holmberg, H. Westerblad, *J. Physiol.* **591**, 3739–3748 (2013).
15. J. Celichowski, K. Grottel, *Acta Neurobiol. Exp. (Warsz.)* **58**, 47–53 (1998).
16. F. E. Zajac, J. L. Young, *J. Neurophysiol.* **43**, 1206–1220 (1980).
17. F. E. Zajac, J. L. Young, *J. Neurophysiol.* **43**, 1221–1235 (1980).

ACKNOWLEDGMENTS

I thank E. Catania for suggesting experimental designs and manuscript comments. This work was supported by a Pradel Award from the National Academy of Sciences, a Guggenheim Fellowship, and NSF grant 0844743. Raw data are available in the supplementary materials.

SUPPLEMENTARY MATERIALS

www.sciencemag.org/content/346/6214/1231/suppl/DC1
Materials and Methods
Supplementary Text
Figs. S1 to S4
Movies S1 to S7

4 September 2014; accepted 13 November 2014
10.1126/science.1260807

INFLAMMATION

Neutrophils scan for activated platelets to initiate inflammation

Vinatha Sreeramkumar,¹ José M. Adrover,¹ Ivan Ballesteros,² Maria Isabel Cuartero,² Jan Rossaint,³ Izaskun Bilbao,^{1,4} Maria Nacher,^{1,5} Christophe Pitaval,¹ Irena Radovanovic,¹ Yoshinori Fukui,⁶ Rodger P. McEver,⁷ Marie-Dominique Filippi,⁸ Ignacio Lizasoain,² Jesús Ruiz-Cabello,^{1,4} Alexander Zarbock,³ María A. Moro,² Andrés Hidalgo^{1,9*}

Immune and inflammatory responses require leukocytes to migrate within and through the vasculature, a process that is facilitated by their capacity to switch to a polarized morphology with an asymmetric distribution of receptors. We report that neutrophil polarization within activated venules served to organize a protruding domain that engaged activated platelets present in the bloodstream. The selectin ligand PSGL-1 transduced signals emanating from these interactions, resulting in the redistribution of receptors that drive neutrophil migration. Consequently, neutrophils unable to polarize or to transduce signals through PSGL-1 displayed aberrant crawling, and blockade of this domain protected mice against thromboinflammatory injury. These results reveal that recruited neutrophils scan for activated platelets, and they suggest that the neutrophils' bipolarity allows the integration of signals present at both the endothelium and the circulation before inflammation proceeds.

Neutrophils are primary effectors of the immune response against invading pathogens but are also central mediators of inflammatory injury (1). Both functions rely on their remarkable ability to migrate within and through blood vessels. The migration of neutrophils is initiated by tethering and rolling on inflamed venules, a process mediated by endothelial selectins (2). Selectin- and chemokine-triggered activation of integrins then allows firm adhesion, after which leukocytes actively crawl on the endothelium before they extravasate or return to the circulation (3). A distinct feature of leukocytes recruited to inflamed vessels is the

rapid shift from a symmetric morphology into a polarized form, in which intracellular proteins and receptors rapidly segregate (4). In this way, neutrophils generate a moving front or leading edge where the constant formation of lamellipodia (actin projections) guides movement, and a uropod or trailing edge where highly glycosylated receptors accumulate (5, 6). We deemed it unlikely that this dramatic reorganization served to exclusively generate a front-to-back axis for directional movement, and we explored the possibility that neutrophil polarization functions as an additional checkpoint during inflammation.

We performed intravital microscopy (IVM) imaging of venules in cremaster muscles of mice treated with the cytokine tumor necrosis factor- α (TNF- α), an inflammatory model in which the vast majority of recruited leukocytes are neutrophils (fig. S1). Within seconds after arresting, leukocytes formed a lamellipodia-rich domain, or leading edge, and a CD62L-enriched uropod, which we could identify by its localization opposite to the leading edge and the direction of cell movement (movie S1 and Fig. 1A) (6–8). Confirming previous reports, we observed numerous interactions of platelets with the leading edge of adherent neutrophils [Fig. 1A and fig. S2A (8–10)]. During these experiments, we noticed that the uropod underwent continuous collisions with circulating platelets, a fraction of which established measurable interactions that were usually transient (Fig. 1B and movie S2). Because platelets captured by the uropod represented a substantial fraction of all interactions (31%), we searched for the receptor(s) mediating these contacts. We reasoned that PSGL-1, a glycoprotein ligand for P-selectin (11) that segregates to the uropod of polarized neutrophils (12), could be responsible for these interactions. Analysis of mice deficient in PSGL-1 (*Selplg*^{-/-} mice) revealed marked reductions in platelet interactions with the uropod, whereas those at the leading edge remained unaffected (Fig. 1B). In contrast, deficiency in the β 2 integrin Mac-1 (*Itgam*^{-/-}) resulted in reductions at both the uropod and leading edge (Fig. 1B). In vivo labeling of Mac-1 and PSGL-1 confirmed these functional data, with Mac-1 localized throughout the cell body and PSGL-1 exclusively at the uropod (Fig. 1C). Specifically, PSGL-1 clustered in a small region of the uropod, whereas CD62L was widely distributed in this domain (Fig. 1C). Analyses of mice expressing a functional Dock2-GFP protein (GFP, green fluorescent protein), a guanine nucleotide exchange factor of Rac GTPases (13), revealed colocalization of Dock2 with PSGL-1 clusters on crawling neutrophils (fig. S3 and movie S3), suggesting active structural dynamics within this region. This observation together with the high frequency of platelet collisions with the PSGL-1 clusters suggested that this domain might be actively protruding into the vessel lumen. Using high-speed spinning-disk

IVM, we could obtain three-dimensional (3D) reconstructions of polarized neutrophils within inflamed venules of Dock2-GFP mice (Fig. 1D), demonstrating that the PSGL-1 clusters indeed projected toward the vessel lumen in about 40% of adherent neutrophils, whereas in the remaining 60% of the cells, it extended laterally, parallel to the endothelial surface (Fig. 1, D and E, and movie S4). As a consequence, the luminal space of inflamed venules was populated by multiple PSGL-1-bearing clusters suitably positioned to interact with circulating cells (Fig. 1F and movie S5).

The observation that only a small fraction of circulating platelets engaged in interactions with the uropod prompted us to search for subsets of platelets prone to this behavior. In vivo labeling for P-selectin or for active β 3 integrins revealed that virtually all platelets interacting with the uropod were activated (P-selectin⁺ or with active β 3 integrins), whereas a fraction of those engaging the leading edge were not (Fig. 1G and figs. S2B and S4). These findings further suggested that P-selectin present on the surface of

activated platelets might be mediating the interactions with the PSGL-1 clusters. Analyses of mice deficient in P-selectin (*Selp*^{-/-} mice) indeed demonstrated patterns of platelet interactions with the two leukocyte subdomains that were similar to those found in mice lacking PSGL-1 (Fig. 1B). These results indicated that neutrophils recruited to inflamed vessels extend a PSGL-1-bearing microdomain into the vessel lumen that scans for activated platelets present in the bloodstream through P-selectin.

During the course of our IVM experiments, we also noticed alterations in the intravascular behavior of adherent neutrophils in the different mutant mice. Deficiency in Mac-1 severely compromised neutrophil crawling on the inflamed vasculature (Fig. 2, A and B), a process previously reported to be mediated by this integrin (3). Surprisingly, although PSGL-1 was excluded from the area of contact with the endothelium (Fig. 1, D and E), neutrophils deficient in this glycoprotein also displayed reductions in crawling displacement and velocity (Fig. 2, A and B),

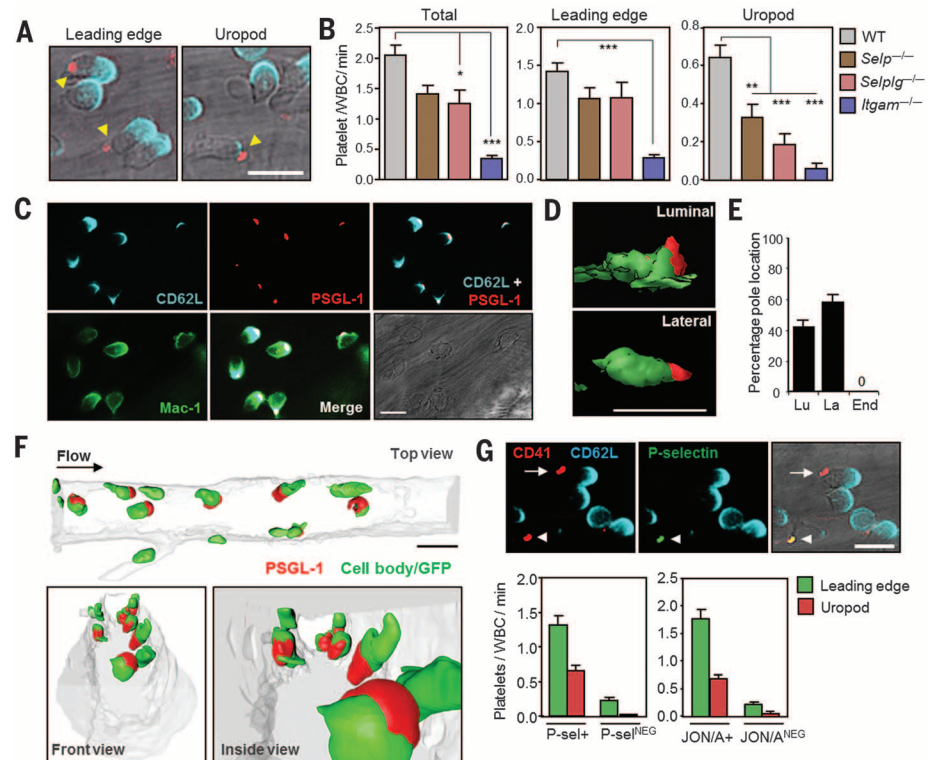


Fig. 1. Neutrophils recruited to inflamed venules interact with activated platelets via protruding PSGL-1 clusters. (A) Micrographs of polarized neutrophils interacting with platelets (red; yellow arrowheads) through the leading edge or the CD62L-labeled uropod (blue). (B) Quantification of total or domain-specific platelet interactions in wild-type mice or mice deficient in P-selectin (*Selp*^{-/-}), PSGL-1 (*Selplg*^{-/-}), or Mac-1 (*Itgam*^{-/-}); $n = 5$ to 8 mice, 38 to 133 interactions. (C) In vivo receptor distribution on polarized wild-type neutrophils. (D) Examples of luminal and lateral projections from 3D reconstructions of polarized Dock2-GFP neutrophils (see also movie S4). (E) Frequency of neutrophils extending PSGL-1 clusters into the lumen (Lu), laterally (La) or between the cell body and the endothelium (En). $n = 6$ mice, 251 cells. (F) 3D reconstructions of an inflamed vessel showing the distribution of PSGL-1 clusters (movie S5). (G) Representative micrographs of neutrophils interacting with nonactivated (arrow) or activated P-selectin⁺ platelets (arrowhead), and quantification of interactions of each domain with P-selectin⁺ or JON/A⁺ platelets. $n = 3$ to 4 mice, 66 to 116 interactions. Scale bars, 10 μ m. Bars show mean \pm SEM. * $P < 0.05$; *** $P < 0.001$, one-way analysis of variance (ANOVA) with Tukey's post-hoc test.

¹Department of Atherothrombosis, Imaging and Epidemiology, Centro Nacional de Investigaciones Cardiovasculares (CNIC), Madrid, Spain. ²Unidad de Investigación Neurovascular, Department of Pharmacology, Faculty of Medicine, Universidad Complutense and Instituto de Investigación Hospital 12 de Octubre (i+12), Madrid, Spain. ³Department of Anesthesiology and Critical Care Medicine, University of Wollongong, New South Wales, Australia. ⁴Ciber de Enfermedades Respiratorias (CIBERES), Madrid, Spain. ⁵Faculty of Science, Medicine and Health, University of Wollongong, New South Wales, Australia. ⁶Division of Immunogenetics, Department of Immunobiology and Neuroscience, Kyushu University, Japan. ⁷Cardiovascular Biology Research Program, Oklahoma Medical Research Foundation, Oklahoma City, OK, USA. ⁸Division of Experimental Hematology and Cancer Biology, Cincinnati Children's Research Foundation, University of Cincinnati College of Medicine, Cincinnati, OH, USA. ⁹Institute for Cardiovascular Prevention, Ludwig-Maximilians-University, Munich, Germany.

*Corresponding author. E-mail: ahidalgo@cnic.es

and these defects were cell-intrinsic (fig. S5 and movie S6). To exclude potential defects originating from PSGL-1 contributions in the early steps of leukocyte recruitment by binding endothelial P-selectin (14), we prevented PSGL-1 binding to P-selectin using a blocking antibody injected after neutrophils had adhered. Inhibition at this stage did not affect leukocyte adhesion to inflamed venules but specifically decreased interactions with the uropod (fig. S6) and caused reductions in crawling kinetics (Fig. 2, A and B). We thus speculated that the engagement of PSGL-1 at the uropod might promote crawling of polarized neutrophils. To test this hypothesis, we first induced transient depletion of platelets, a treatment that resulted in virtual suppression of crawling (Fig. 2, A and B, and fig. S7A). We next analyzed two models in which neutrophil polarization or signaling through PSGL-1 was impaired. In the first model, we induced hematopoietic-specific deletion of the gene encoding *Cdc42* (fig. S8A), a small Rho-GTPase required for neutrophil polarization (15). Confirming previous *in vitro* observations, *Cdc42*-deficient neutrophils were unable to form a leading edge-to-uropod axis and instead formed multiple protrusions, lacked a distinguishable uropod, and failed to form PSGL-1 clusters *in vivo* (fig. S8B). Impaired polarization in these mutants compromised interactions between neutrophils and circulating platelets (fig. S8C), and neutrophils in these mice displayed severely impaired crawling kinetics (Fig. 2, C and D). In the second model, we analyzed mice in which PSGL-1 is normally distributed at the cell surface and can interact with P-selectin but cannot propagate outside-in signals because of the absence of the cytoplasmic domain [PSGL-1^{ΔCyt} mice (16)]. Although neutrophil adhesion to TNF- α -stimulated vessels was partially compromised in PSGL-1^{ΔCyt} mice because of reductions in the surface levels of PSGL-1, those cells that adhered polarized normally (fig. S9A) and displayed marked reductions in crawling kinetics (Fig. 2, C and D) despite elevated levels of Mac-1 on the surface (fig. S9B). Thus, polarization of a signaling-competent PSGL-1 drives the intravascular migration of neutrophils.

To search for possible mechanisms by which PSGL-1-derived signals promoted crawling, we analyzed the *in vivo* distribution of Mac-1 and the chemokine receptor CXCR2, two receptors required for the intravascular migration of neutrophils (3, 17). In wild-type cells, Mac-1 was homogeneously distributed throughout the cell body, whereas CXCR2 preferentially localized at the leading edge (Fig. 2E and movie S7). Neutrophils deficient in PSGL-1 exhibited a mislocalization of both receptors (Fig. 2E, fig. S10, and movie S8). These alterations were even more dramatic in wild-type mice upon platelet depletion (figs. S7B and S10 and movie S9), which agreed with the suppression of crawling in these mice (Fig. 2A). The absence or inhibition of PSGL-1 in Mac-1-deficient mice did not lead to further reductions in platelet interactions or crawling kinetics (fig. S11), indicating that these receptors function along the same pathway and

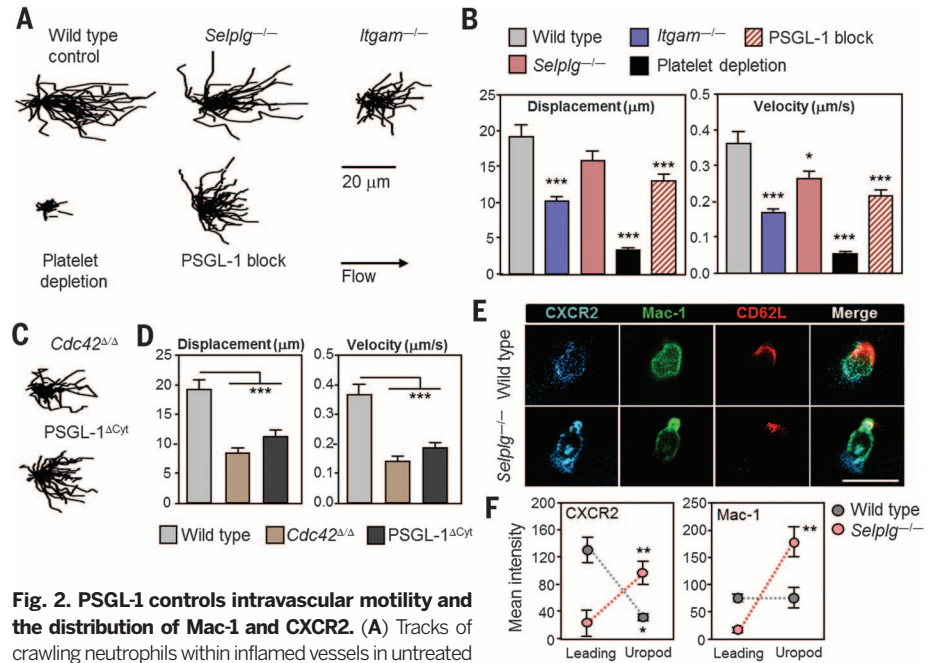


Fig. 2. PSGL-1 controls intravascular motility and the distribution of Mac-1 and CXCR2.

(A) Tracks of crawling neutrophils within inflamed vessels in untreated wild-type mice, mice deficient in PSGL-1 (*Selplg*^{-/-}) or Mac-1 (*Itgam*^{-/-}), and mice depleted of platelets by antiplatelet serum or treated with a PSGL-1-blocking antibody. (B) Quantification of the crawling displacements and instantaneous velocities of neutrophils in the same groups as (A); *n* = 50 to 56 cells, 4 to 9 mice. (C) Tracks of neutrophils with conditional deletion of *Cdc42* or expressing a mutant form of PSGL-1 that lacks the cytoplasmic tail (PSGL-1^{ΔCyt}) and (D) quantification of the displacement per minute and instantaneous velocities of adhered neutrophils. *n* = 50 to 55 cells, 3 to 5 mice. (E) Representative micrographs and quantification (F) of the *in vivo* distribution of CXCR2 and Mac-1 in polarized neutrophils from wild-type and PSGL-1-deficient mice; *n* = 17 to 19 cells, 3 mice. Scale bar, 10 μ m. Data show mean \pm SEM. **P* < 0.05; ***P* < 0.01; ****P* < 0.001; ANOVA with Tukey's multigroup test (B) or unpaired *t* test (F).

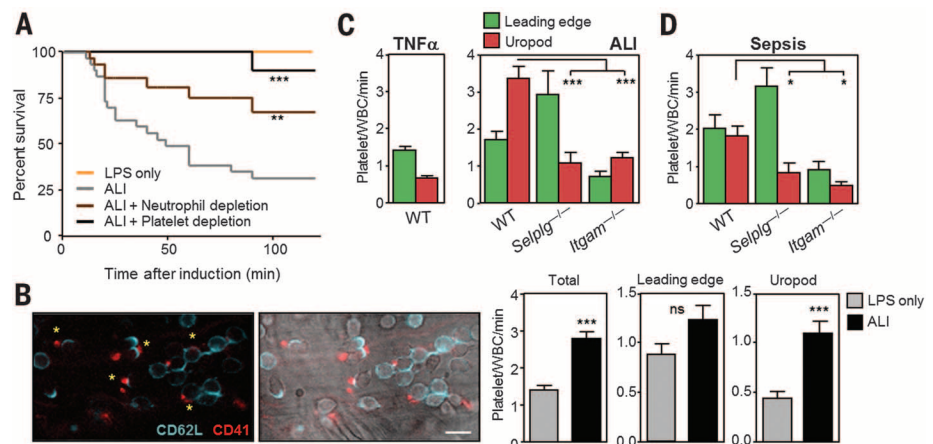
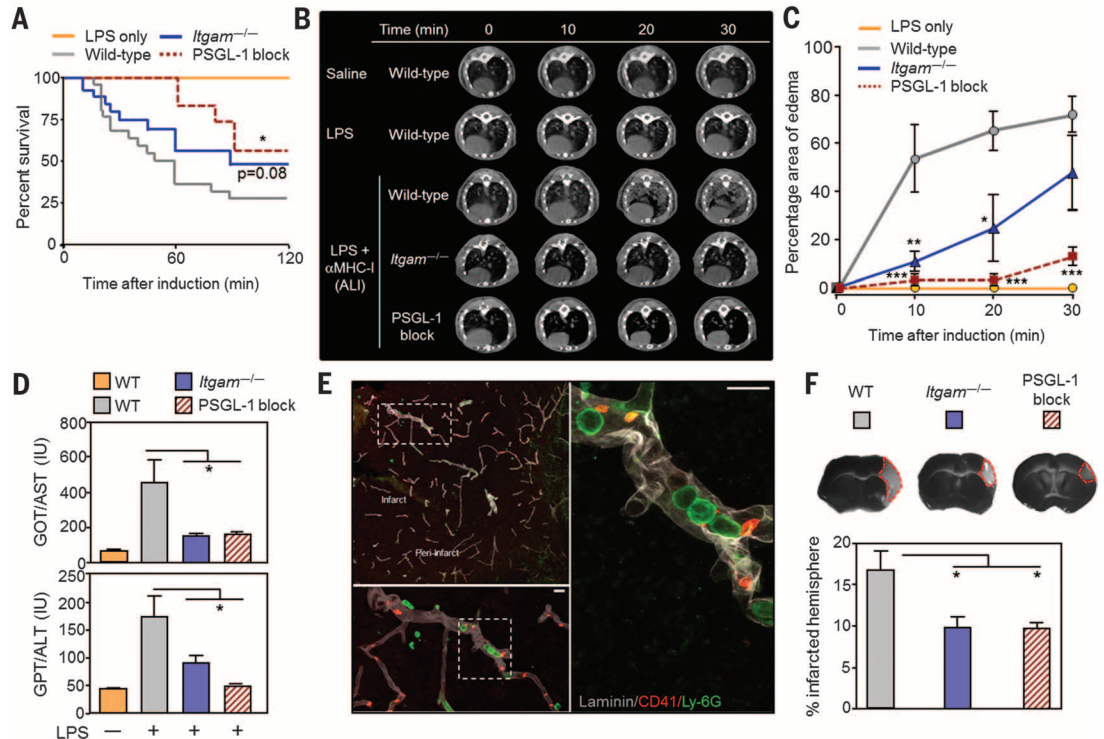


Fig. 3. PSGL-1 at the uropod becomes a preferred docking site for platelets during pathological inflammation.

(A) Survival curves of Balb/c mice treated with lipopolysaccharide (LPS) alone or LPS plus anti-MHC-1 (MHC, major histocompatibility complex) to induce ALI. Neutrophils were depleted using anti-Ly6G, and platelets using antiplatelet serum before the induction of ALI; *n* = 5 to 20 mice. (B) (Left) Representative micrographs of inflamed venules during ALI. The asterisks indicate platelets interacting with the uropod of neutrophils. (Right) Quantification of platelet interactions with the leading edge or uropod in control (LPS only) and ALI-induced mice. Scale bar, 10 μ m. *n* = 3 to 4 mice, 32 to 73 interactions. (C) Frequency of interactions with the leading edge or uropod in TNF- α -treated or ALI-induced mice, and distribution of interactions in wild-type mice and mice deficient in PSGL-1 (*Selplg*^{-/-}) or Mac-1 (*Itgam*^{-/-}); *n* = 3 to 5 mice, 23 to 137 interactions. (D) Frequency of interactions with the leading edge or uropod during sepsis in wild-type mice and mice deficient in PSGL-1 or Mac-1. *n* = 3 to 4 mice, 32 to 56 interactions. Bars show mean \pm SEM. **P* < 0.05; ****P* < 0.001 as determined by ANOVA with Tukey's multigroup test.

Fig. 4. PSGL-1-mediated interactions trigger vascular injury.

(A) Survival curves of Balb/c mice treated with LPS alone or LPS plus anti-MHC-1 to induce ALI. The absence of Mac-1 or inhibition of PSGL-1 protects from death; $n = 5$ to 19 mice. **(B)** Representative axial slices of the thorax of Balb/c mice at different times after induction of ALI. The white signal in the pulmonary space identifies edema, which is quantified in **(C)**; $n = 7$ to 8 mice per group. **(D)** Quantification of hepatic injury as levels of AST and ALT transaminases in plasma of the indicated group of mice 24 hours after treatment with LPS; $n = 7$ to 11 mice. **(E)** Representative brain sections of wild-type mice 24 hours after inducing ischemia, showing vessels at increasing magnifications and intra-vascular neutrophil (Ly6G, green)–platelet (CD41, red) aggregates. Scale bars, 10 μm . **(F)** Percentages of infarcted hemispheres 24 hours after arterial occlusion in control wild-type mice, mice deficient in Mac-1 (*Itgam*^{-/-}), and wild-type mice after blocking PSGL-1. Images are representative brain sections stained with TTC, showing the extent of ischemia as white areas with a red outline; $n = 5$ to 8 mice. Bars show mean \pm SEM. * $P < 0.05$; ** $P < 0.01$; *** $P < 0.001$, ANOVA with Tukey's multigroup test.



that additional platelet-derived mediators and unknown neutrophil receptors that mediate platelet interactions can regulate crawling. Thus, intact distribution of and signaling through PSGL-1 at the uropod regulates neutrophil crawling, at least in part by orchestrating the appropriate distribution of adhesive and chemotactic receptors.

We next explored how this phenomenon might contribute to pathogenic inflammation. We used a model of acute lung injury (ALI) in Balb/c mice that closely simulates transfusion-related ALI (18). In this model, the transient elimination of neutrophils or platelets protects from death [Fig. 3A and (19)], indicating that this might be an appropriate model to study the functional partnership between these cells. Intravital analyses of the cremaster microvessels in ALI-induced mice confirmed the findings in crawling kinetics, receptor distribution, and luminal or lateral projections made using TNF- α (fig. S12 and movie S10) and further revealed that during ALI, the uropod becomes the predominant domain for platelet interactions, which contrasted with the preferred use of the leading edge in the non-pathogenic TNF- α -induced model (Fig. 3, B and C). Interactions at the uropod during ALI were mediated by PSGL-1, whereas Mac-1 mediated interactions with both domains (Fig. 3C and fig. S13). We obtained similar responses in a model of endotoxemia (Fig. 3D), indicating that during pathological inflammation, the uropod becomes the dominant interacting domain for circulating platelets.

To test whether the engagement of PSGL-1 at the uropod was causally related to neutrophil-mediated vascular inflammation, we explored its contribution in the model of ALI. Intravital imaging of the pulmonary microcirculation revealed a rapid increase in platelets captured by recruited neutrophils that were strongly inhibited by blocking PSGL-1 (fig. S14). In addition, deficiency in PSGL-1 or Mac-1, or inhibition of PSGL-1, resulted in moderate protection from ALI-induced death (Fig. 4A and fig. S15A). The use of computed tomography to track pulmonary edema over time revealed partial protection from ALI in mice deficient in Mac-1 and almost complete protection when PSGL-1 interactions were blocked (Fig. 4, B and C). This protection correlated with reduced neutrophil infiltrates in the lung (fig. S16) and suggested that interactions at the uropod critically contribute to vascular injury. Deficiency in either receptor or inhibition of PSGL-1 also prevented hepatic damage during endotoxemia (Fig. 4D and fig. S15B). Consistent with previous reports (20, 21), we detected elevations in the plasma levels of neutrophil-derived extracellular traps (NETs) during ALI and sepsis. These elevations were completely blunted when platelets were depleted, by blocking PSGL-1, or in the absence of Mac-1 (fig. S17), suggesting that other forms of neutrophil activation can be triggered upon platelet interactions through PSGL-1.

Finally, we examined whether PSGL-1-mediated interactions also underlie ischemic injury, a prev-

alent form of vascular disease (22). We used a model of stroke triggered by permanent occlusion of the middle cerebral artery, in which neutrophil depletion significantly reduces tissue death as measured by the percentage of infarcted hemisphere [fig. S18 and (23)]. Interactions between neutrophils and platelets within the microvasculature of infarcted brains were inhibited by blocking PSGL-1 (Fig. 4E and fig. S19), and this correlated with significant reductions in infarct volumes when PSGL-1 was inhibited or in the absence of Mac-1 (Fig. 4F).

We have uncovered a critical checkpoint during the early stages of inflammation: Neutrophils recruited to injured vessels extend a domain into the lumen, where PSGL-1 clusters scan for the presence of activated platelets. Only when productive interactions occur do neutrophils organize additional receptors needed for intravascular migration or generate NETs, and inflammation ensues (fig. S20 and movie S11). Our findings reveal that the dynamic reorganization of neutrophil domains and receptors allows simultaneous interactions with both the vascular wall and activated platelets in the circulation to provide a rapid and efficient regulatory mechanism early during inflammation.

REFERENCES AND NOTES

1. M. Phillipson, P. Kubes, *Nat. Med.* **17**, 1381–1390 (2011).
2. K. Ley, C. Laudanna, M. I. Cybulsky, S. Nourshargh, *Nat. Rev. Immunol.* **7**, 678–689 (2007).
3. M. Phillipson et al., *J. Exp. Med.* **203**, 2569–2575 (2006).

4. K. F. Swaney, C. H. Huang, P. N. Devreotes, *Annu. Rev. Biophys.* **39**, 265–289 (2010).
5. A. J. Ridley *et al.*, *Science* **302**, 1704–1709 (2003).
6. F. Sánchez-Madrid, J. M. Serrador, *Nat. Rev. Mol. Cell Biol.* **10**, 353–359 (2009).
7. For more details on this and other procedures, please refer to the Materials and Methods section in the Supplemental Materials.
8. A. Hidalgo *et al.*, *Nat. Med.* **15**, 384–391 (2009).
9. J. W. Sempke, J. E. Italiano Jr., J. Freedman, *Nat. Rev. Immunol.* **11**, 264–274 (2011).
10. M. L. von Brühl *et al.*, *J. Exp. Med.* **209**, 819–835 (2012).
11. K. L. Moore *et al.*, *J. Cell Biol.* **128**, 661–671 (1995).
12. E. Y. Chiang, A. Hidalgo, J. Chang, P. S. Frenette, *Nat. Methods* **4**, 219–222 (2007).
13. Y. Kunisaki *et al.*, *J. Cell Biol.* **174**, 647–652 (2006).
14. A. Zarbock, K. Ley, R. P. McEver, A. Hidalgo, *Blood* **118**, 6743–6751 (2011).
15. K. Szczur, Y. Zheng, M. D. Filippi, *Blood* **114**, 4527–4537 (2009).
16. J. J. Miner *et al.*, *Blood* **112**, 2035–2045 (2008).
17. B. McDonald *et al.*, *Science* **330**, 362–366 (2010).
18. M. R. Looney, B. M. Gilliss, M. A. Matthay, *Curr. Opin. Hematol.* **17**, 418–423 (2010).
19. M. R. Looney *et al.*, *J. Clin. Invest.* **119**, 3450–3461 (2009).
20. A. Caudrillier *et al.*, *J. Clin. Invest.* **122**, 2661–2671 (2012).
21. S. R. Clark *et al.*, *Nat. Med.* **13**, 463–469 (2007).
22. G. A. Donnan, M. Fisher, M. Macleod, S. M. Davis, *Lancet* **371**, 1612–1623 (2008).
23. M. I. Cuartero *et al.*, *Stroke* **44**, 3498–3508 (2013).

ACKNOWLEDGMENTS

We thank G. Crainiciuc, J. A. Quintana, I. Ortega, and A. Santos for technical support and D. Sancho and S. González for insightful comments. The data presented in this manuscript can be found in the main paper and supplementary materials. This study was supported by NIH grants HLO3463, HL085607 (R.P.M.), and HL090676 (M.-D.F.); German Research Foundation grants ZA428/8-1, ZA428/6-1, and SFB 1009-TP A05 (A.Z.); FP7 Marie Curie (ITN-264864; π -net) and S2010/BMD-2326 from Comunidad de Madrid (J.R.-C.); Grants-in-Aid for Scientific Research from the Japan Society for the Promotion of Science (Y.F.); CSD2010-00045 and SAF2012-33216 from Ministerio de Economía y Competitividad (MINECO) and S2010/BMD-2336 from

Comunidad de Madrid (M.A.M.); and a Ramón y Cajal Fellowship (RYC-2007-00697), SAF2009-11037 and 2012-31142 from MINECO, S2010/BMD-2314 from Comunidad de Madrid, and 246655 from FP7-People-IRG Program (A.H.). The CNIC is supported by the MINECO and the Pro-CNIC Foundation. R.P.M. is cofounder of Selexys Pharmaceuticals, which is developing monoclonal antibodies to PSGL-1 and P-selectin to treat inflammatory and thrombotic diseases. A patent application for the blockade of PSGL-1 in thromboinflammation has been filed by V.S. and A.H. (EP14382425.8). The authors declare no other conflicts of interest.

SUPPLEMENTARY MATERIALS

www.sciencemag.org/content/346/6214/1234/suppl/DC1
Materials and Methods
Figs. S1 to S20
Tables S1 and S2
References (24–29)
Movies S1 to S11

27 May 2014; accepted 7 November 2014
10.1126/science.1256478

TRANSCRIPTION

Chromatin decondensation is sufficient to alter nuclear organization in embryonic stem cells

Pierre Therizols, Robert S. Illingworth, Celine Courilleau, Shelagh Boyle, Andrew J. Wood, Wendy A. Bickmore*

During differentiation, thousands of genes are repositioned toward or away from the nuclear envelope. These movements correlate with changes in transcription and replication timing. Using synthetic (TALE) transcription factors, we found that transcriptional activation of endogenous genes by a viral trans-activator is sufficient to induce gene repositioning toward the nuclear interior in embryonic stem cells. However, gene relocation was also induced by recruitment of an acidic peptide that decondenses chromatin without affecting transcription, indicating that nuclear reorganization is driven by chromatin remodeling rather than transcription. We identified an epigenetic inheritance of chromatin decondensation that maintained central nuclear positioning through mitosis even after the TALE transcription factor was lost. Our results also demonstrate that transcriptional activation, but not chromatin decondensation, is sufficient to change replication timing.

Radial nuclear organization of the genome is conserved in eukaryotes (1), with an accumulation of heterochromatin, gene-poor and late-replicating chromatin domains found near the nuclear envelope (2). Lamin-associated domains (LADs) are gene-poor, show low levels of transcription, and are depleted for active histone marks (3). Artificial tethering to the nuclear envelope has demonstrated that a peripheral nuclear environment is sufficient to induce transcriptional down-regulation of both reporter genes and some endogenous genes in somatic cells (4, 5), and during differentiation many genes change their association with components of the nuclear lamina—often correlated

with altered gene expression (6). However, these correlations do not determine whether relocation relative to the nuclear periphery is a cause or a consequence of gene regulation during differentiation.

Two-thirds of the genes that lose lamin B1 association during differentiation of embryonic stem cells (ESCs) to neural precursor cells (NPCs) are transcriptionally up-regulated. The others are more likely to be strongly activated later in differentiation (6). *Ptn*, *Sox6*, and *Nrp1* are three genes that are up-regulated during ESC differentiation (7); they exhibit some of the largest losses of lamin B1 association during ESC-to-NPC differentiation (6) and, concomitantly, *Ptn* loses its peripheral nuclear position (8). The expression of *Ptn* and *Nrp1* begins to increase as ESCs differentiate into epiblast stem cells (EpiSCs) (Fig. 1B). Although there are no data on LADs in EpiSCs, fluorescence in situ hybridization

(FISH) showed that *Ptn*, *Sox6*, and *Nrp1* loci relocate away from the nuclear periphery and toward more central nuclear positions, correlated to their expression changes, during the differentiation of ESCs to EpiSCs or to NPCs ($P < 0.01$; Fig. 2B and fig. S1).

To directly address the role of transcription in nuclear reorganization, we ectopically activated *Ptn*, *Sox6*, or *Nrp1* in ESCs by means of synthetic transcription factors composed of TALE (transcription activator–like effector) DNA binding domains with specificity for the respective gene promoters (9) fused to VP64, a tetramer of the VP16 acidic transcriptional activator (10, 11) (Fig. 1A). When transfected into ESCs, tPtn-VP64 induced expression of its target by a factor of >30 to 90 (Fig. 1, B and C). Other than *Ptn*, only two additional genes (*Il33* and *Nnmt*) were significantly up-regulated, and genes involved in ESC pluripotency or differentiation were not significantly changed. This suggests that *Ptn* up-regulation is not just an indirect consequence of differentiation triggered by transfection or the nonspecific expression of an acidic activator (Fig. 1C and fig. S2). Specific activation of *Nrp1* or *Sox6* in cells transfected by tNrp1-VP64 or tSox6-VP64, respectively, also showed no expression signature of differentiation (Fig. 1B). Control plasmids lacking the VP64 domain (tPtn- Δ , tSox6- Δ , and tNrp1- Δ) had almost no effect (Fig. 1, B and C). Moreover, we did not detect any changes in the expression of genes neighboring those targeted by the TALEs (Fig. 1C and fig. S3).

As well as activating *Ptn*, *Nrp1*, or *Sox6*, FISH showed that tPtn-VP64, tNrp1-VP64, and tSox6-VP64 caused specific relocalization of the targeted loci toward the center of ESC nuclei, relative to control [enhanced green fluorescent protein (eGFP)] transfection (tPtn-VP64, $P = 4.6 \times 10^{-9}$; tNrp1-VP64, $P = 5.3 \times 10^{-14}$; tSox6-VP64, $P = 6.4 \times 10^{-12}$) or to constructs lacking the activation domain (tPtn- Δ , $P = 3 \times 10^{-6}$; tNrp1- Δ , $P = 8.1 \times 10^{-10}$; tSox6- Δ , $P = 8 \times 10^{-12}$) (Fig. 2, A and B). The extent of this relocalization was similar to that seen upon normal

MRC Human Genetics Unit, Institute of Genetics and Molecular Medicine, University of Edinburgh, Crewe Road, Edinburgh EH4 2XU, UK.

*Corresponding author. E-mail: wendy.bickmore@igmm.ed.ac.uk



Neutrophils scan for activated platelets to initiate inflammation

Vinatha Sreeramkumar *et al.*

Science **346**, 1234 (2014);

DOI: 10.1126/science.1256478

This copy is for your personal, non-commercial use only.

If you wish to distribute this article to others, you can order high-quality copies for your colleagues, clients, or customers by [clicking here](#).

Permission to republish or repurpose articles or portions of articles can be obtained by following the guidelines [here](#).

The following resources related to this article are available online at www.sciencemag.org (this information is current as of December 4, 2014):

Updated information and services, including high-resolution figures, can be found in the online version of this article at:

<http://www.sciencemag.org/content/346/6214/1234.full.html>

Supporting Online Material can be found at:

<http://www.sciencemag.org/content/suppl/2014/12/03/346.6214.1234.DC1.html>

This article **cites 28 articles**, 13 of which can be accessed free:

<http://www.sciencemag.org/content/346/6214/1234.full.html#ref-list-1>